Coherent Ballistic Motion of Electrons in a Periodic Potential

W. Kuehn,[1] P. Gaal,[1] K. Reimann,[1] M. Woerner,[1] T. Elsaesser,[1] and R. Hey[2]

[1]*Max-Born-Institut für Nichtlineare Optik und Kurzzeitspektroskopie, 12489 Berlin, Germany*
[2]*Paul-Drude-Institut für Festkörperelektronik, 10117 Berlin, Germany*

Electrons in bulk *n*-doped GaAs at a lattice temperature of 300 K are driven by ultrashort high-field
transients of up to 300 kV/cm in the terahertz frequency range. In the lowest conduction band the carriers
show coherent ballistic motion, which is detected via the THz field emitted by them. This partial Bloch
oscillation is reproduced by a quantum-kinetic theory of coherent transport on ultrafast time scales.

Eighty years ago, Felix Bloch showed that electron wave functions in the Coulomb potential of the nuclei in a crystal are periodically modulated plane waves [1]. The spatially periodic modulation of these Bloch functions restricts the allowed energies of the electrons, leading to a dispersive band structure $\mathcal{E}(\hbar\vec{k})$ containing both allowed (bands) and forbidden energy regions (gaps) [2]. Without scattering, an electron (charge $-e$) in an electric field $\vec{E}$ is expected to follow the dispersion of its band at a constant rate in momentum space [3],

$$\hbar \, d\vec{k}/dt = -e\vec{E}. \qquad (1)$$

The corresponding velocity $\vec{v}$ in real space is given by

$$\vec{v} = \hbar^{-1}\nabla_{\vec{k}}\mathcal{E}(\hbar\vec{k}). \qquad (2)$$

Thus, an electron moving in the periodic Coulomb potential of a crystal under the action of a constant external electric field is expected to undergo a coherent periodic oscillation both in real and momentum space. So far, such Bloch oscillations [1] have been observed only in artificial systems such as semiconductor superlattices [4], atoms and/or Bose-Einstein condensates in optical lattices [5], Josephson junction arrays [6], or optical waveguide arrays [7]. The absence of Bloch oscillations in electron transport through bulk crystals is attributed to efficient scattering of electrons on a sub-100 fs time scale, a prediction of the semiclassical Boltzmann transport equation (BTE) [8].

The BTE includes scattering rates described by two important time constants, the energy relaxation time $\tau_{\mathcal{E}}$, the average time in which a carrier loses its kinetic energy, and the momentum relaxation time τ_p [see Fig. 1(a)]. Elastic scattering contributes to τ_p but not to $\tau_{\mathcal{E}}$ and, thus, $\tau_p < \tau_{\mathcal{E}}$. In the most basic approach, τ_p and $\tau_{\mathcal{E}}$ are derived from Fermi's golden rule (FGR) with the respective scattering matrix element and the density of final states being the key quantities. For electric fields varying slower than $\tau_{\mathcal{E}}$ the BTE predicts stationary drift transport with a field-dependent drift velocity [Fig. 1(b)]. For fields varying faster than τ_p, the BTE predicts ballistic transport according to Eq. (1). In the intermediate regime [Fig. 1(a)], phenomena like incoherent (driftlike) velocity overshoot

occur with the velocity being in phase with the driving field.

As shown in Fig. 1(a), the FGR approach including all types of electron-phonon scattering in bulk GaAs predicts a strong decrease of the momentum relaxation time τ_p with increasing field [8]. For $E \approx 300$ kV/cm, a value of $\tau_p \approx 3$ fs is found, restricting the regime of ballistic transport, the prerequisite for Bloch oscillations, to negligibly small times. The prediction of such short momentum relaxation times is, however, beyond the validity of FGR, since FGR is only applicable if the time interval between two scattering events is long compared to the duration of a scattering
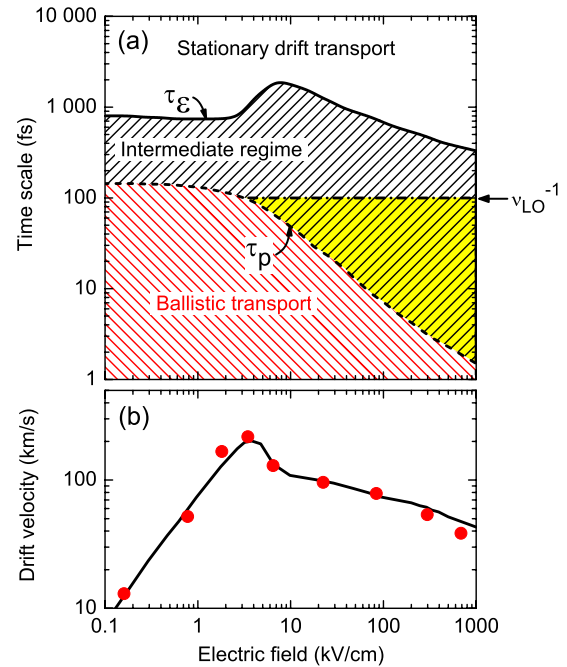

FIG. 1 (color online). (a) Regimes of high-field transport in GaAs as a function of the applied electric field. The energy ($\tau_{\mathcal{E}}$) and momentum (τ_p) relaxation times are taken from the BTE [8]. The quantum-kinetic regime (gray/yellow triangle) lies between τ_p and the inverse LO phonon frequency ν_{LO}^{-1}. (b) Stationary drift velocity (symbols: dynamic polaron theory, solid line: BTE) vs electric field. The Gunn effect [21] occurs in the range of negative slope $E > 3$ kV/cm.

event. For electron-phonon interaction, optical phonon scattering represents the shortest event with a duration of the order of $\nu_{LO}^{-1} = 115$ fs, much longer than 3 fs. Thus, a realistic picture of electron transport at high fields requires a quantum-kinetic treatment for times $t < \nu_{LO}^{-1}$ [Fig. 1(a)]. In the ballistic range $t < \tau_p$, the quantum-kinetic and the BTE description give identical results.

In this Letter, we demonstrate a novel regime of electron transport in bulk crystals driven by ultrashort high-field transients in the terahertz (THz) frequency range with electric-field amplitudes of up to 300 kV/cm. Electrons in a thin n-doped GaAs crystal show a coherent ballistic motion within the lowest conduction band, in this way performing a partial Bloch oscillation that explores halfway to the boundary of the first Brillouin zone. We analyze the experimental results with a dynamic polaron model, reproducing the observed behavior.

One can investigate experimentally the quantum-kinetic regime of carrier transport [gray/yellow triangle in Fig. 1(a)] by applying a strong electric field, $E \gg 10$ kV/cm, on a very short time scale, i.e., $\omega_{THz}^{-1} \ll 200$ fs, and by simultaneously monitoring the transient position of the electron in k space. In our experiments, we apply THz transients with $\omega_{THz}^{-1} \approx 80$ fs and $20 < E < 300$ kV/cm to electrons in a GaAs crystal and monitor their transient velocity [Eq. (2)] via the coherent THz radiation emitted by the carriers. The sample investigated was grown by molecular beam epitaxy and consists of a 500 nm thin layer of Si-doped (donor concentration $N_D = 2 \times 10^{16}$ cm^{-3}) GaAs clad between two 300 nm thin Al$_{0.4}$Ga$_{0.6}$As layers [9]. A few-cycle THz pulse with a center frequency of 2 THz, generated by optical rectification of 25 fs pulses from a Ti:sapphire oscillator-amplifier laser system, excites the sample placed in the focus of a parabolic mirror. The direction of the electric field is along the [100] direction of the sample. With a further pair of parabolic mirrors the electric field of the transmitted THz pulse is transferred to a thin ZnTe crystal, where it is measured via electro-optic sampling (our setup is the THz part of the setup shown in Fig. S1 of [10]). The optics used ensures that, apart from a sign change, the electric-field transients at the sample and at the electro-optic crystal are identical. The entire optical path of the THz beam is placed in vacuum. The electron current density [11],

$$j(t) = -en\upsilon(t) = -2E_{em}(t)/(Z_0 d), \qquad (3)$$

in the sample is proportional to the coherently emitted field $E_{em}(t) = E_{tr}(t) - E_{in}(t)$, the difference of $E_{tr}(t)$, the field transmitted through the sample, and $E_{in}(t)$, the field incident on the sample (n, electron density in the sample, $Z_0 = \mu_0 c = 377\ \Omega$, the impedance of free space). As the thickness of our sample $d = 500$ nm is much less than the THz wavelength $\lambda \approx 150\ \mu$m, all electrons in the sample experience the same driving field $E_{tr}(t)$ [12].

Our setup differs from the often used setup [13] where a large area of the sample is imaged as a small focal spot on

the electro-optic crystal. In the latter case the electric field measured at the electro-optic crystal is proportional to the time derivative of the electric field at the sample.

In Figs. 2 and 3 we present experimental results at a sample temperature of 300 K for incident THz pulses with various amplitudes. Figure 2(a) and 2(b) show the transients of the incident $E_{in}(t)$ and of the transmitted $E_{tr}(t)$ pulses for an amplitude of 300 kV/cm. The difference between these transients yields the field $E_{em}(t)$ emitted by the sample and the electron velocity [Eq. (3)], shown in Fig. 2(c). The noise level of the experimental data for $E_{em}(t)$ is 0.5 kV/cm. Part (d) shows $-k(t)$ calculated according to Eq. (1) from $E_{tr}(t)$. Plotting $\upsilon(t)$ from Fig. 2(c) versus $-k(t)$ from Fig. 2(d) one obtains the dots in (f). To
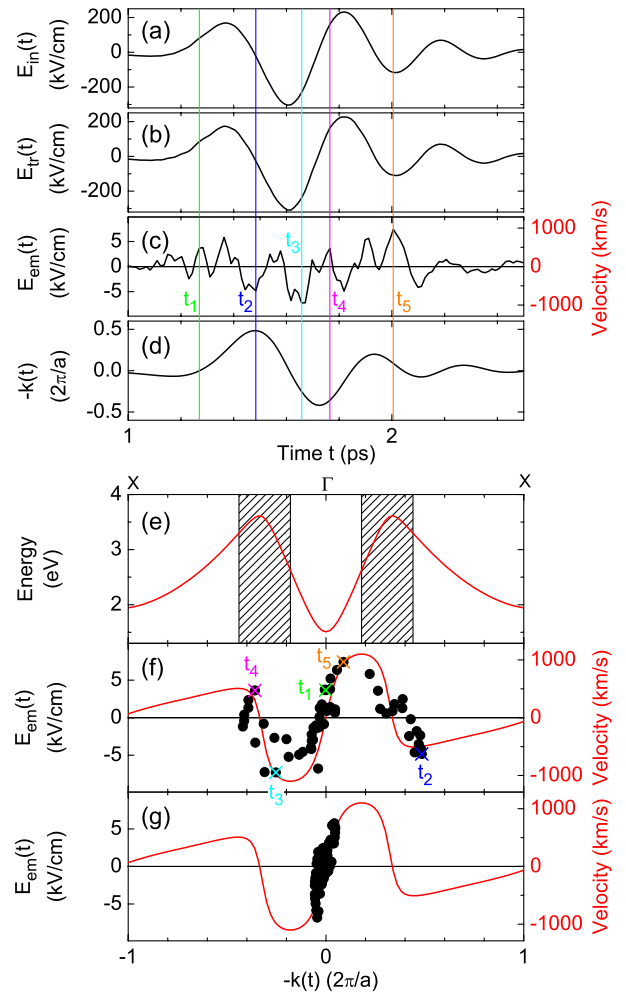

FIG. 2 (color online). (a) Measured incident electric field as a function of time, $E_{in}(t)$. (b) Electric field transmitted through the sample, $E_{tr}(t)$. (c) Emitted electric field, $E_{em}(t)$. (d) $-k(t)$ obtained from Eq. (1), in units of $2\pi/a$. (e) Lowest conduction band of GaAs in [100] direction. The negative mass regions are hatched [2]. (f) Dots, $E_{em}(t)$ plotted versus $-k(t)$. Crosses show the values at the times t_1 to t_5, marked by vertical lines in (a) to (d). Solid line, velocity υ calculated using Eq. (2). (g) Same plot as in (f), but for an electric-field amplitude of 50 kV/cm [see Fig. 3(b)].
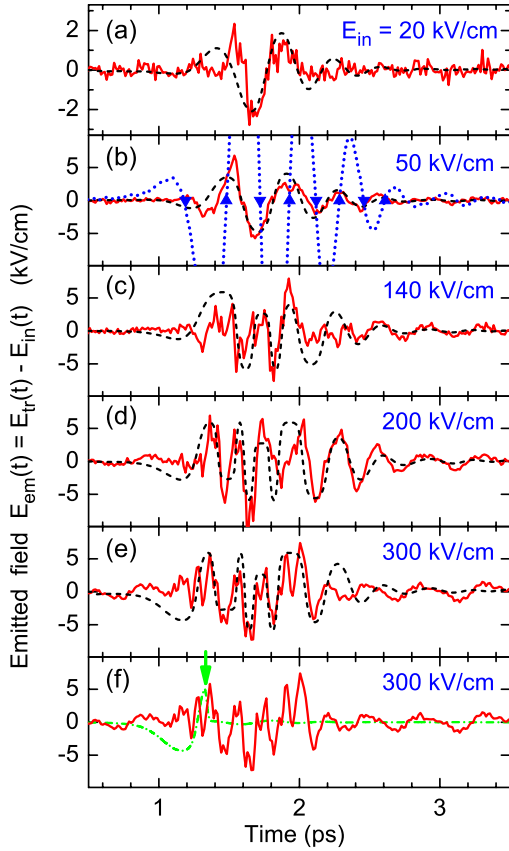
FIG. 3 (color online). Solid lines: emitted field transients $E_{em}(t)$ for different amplitudes of the incident electric field. The data in (e) and (f) are the same as in Fig. 2(c). Dashed lines in (a) to (e): results of the model calculation based on the band structure of GaAs. The dotted line and triangles in (b) show the driving field and its zero-crossings. (f) Same experimental data as in (e), now compared to the results (dash-dotted line) of a calculation assuming the intervalley scattering rates of [8]. At the time marked by the arrow the electrons can scatter into the side valleys.

clarify the origin of the dots in (f), we have marked five moments t_1 to t_5. Comparing these experimental results with the v vs k relationship [solid line in (f), Eq. (2)] from the conduction band (e), one finds a good agreement, pointing to ballistic transport across half the Brillouin zone. For lower incident electric-field amplitudes [Fig. 2(g)] we explore a much smaller part of the Brillouin zone.

To illustrate the effect of the band structure on the electron velocity consider the time between t_2 and t_3. During this period, the electric field acting on the electron is negative [Fig. 2(b)]. The electron velocity is negative at t_2, then gets positive, and then gets negative again [Fig. 2(c)]. Thus, although the electric field has the same direction between t_2 and t_3, there are times with positive and times with negative acceleration, showing that the effective mass of the electron changes sign. The effective mass of a band electron is given by the curvature of its band, $m_{eff} = \hbar^2[d^2\mathcal{E}(\hbar k)/dk^2]^{-1}$. In the conduction band of GaAs, the effective mass is positive around the Γ and the

X points and negative around the band maxima [hatched areas in Fig. 2(e)], explaining the change of the sign of the acceleration between t_2 and t_3. Even as late as t_5, the data still agree with the velocity-momentum relationship expected for ballistic transport. Our interpretation of the results is in agreement with the experimental data for all THz electric-field amplitudes measured (solid lines in Fig. 3). The dashed curves are calculated assuming ballistic transport according to Eq. (1). For drift transport, the electron velocity $v(t) \propto E_{em}(t)$ would be in phase with the driving field $E_{tr}(t)$ [dotted line in Fig. 3(b)]. We find, however, that the zero crossings of $E_{tr}(t)$ (triangles) coincide with the maxima (minima) of $E_{em}(t)$ demonstrating a $90°$ phase-delayed velocity, a direct evidence for ballistic transport. Increasing the field amplitude [Figs. 3(c)–3(e)], we observe higher-frequency components and a clipping of the emitted field amplitude around $|E_{em}(t)| < 7$ kV/cm. Since the emitted field is proportional to the electron velocity [Eq. (3)], this clipping is caused by the maximum velocity possible in the conduction band [Fig. 2(f)].

Now, we compare our experimental findings with two different theoretical approaches, both based on the same Hamiltonian in the single-electron picture [14], including the conduction band structure $\mathcal{E}(\hbar\vec{k})$ [2] and the interaction with the external field $E(t)$ in x direction:

$$H(t) = \mathcal{E}(\vec{p}) - exE(t) + \sum_{b,\vec{q}} \frac{P_{b,\vec{q}}^2 + \omega_{b,\vec{q}}^2 Q_{b,\vec{q}}^2}{2}$$

$$+ \sum_{b,\vec{q}} M_{b,\vec{q}}[P_{b,\vec{q}} \cos\vec{q}\,\vec{r} + \omega_{b,\vec{q}} Q_{b,\vec{q}} \sin\vec{q}\,\vec{r}]. \quad (4)$$

$\vec{r}$ and $\vec{p}$ are position and momentum of the electron, $Q_{b,\vec{q}}$ and $P_{b,\vec{q}}$ are the coordinate and the conjugate momentum of the phonon of branch b with wave vector $\vec{q}$ and frequency $\omega_{b,\vec{q}}$, and the $M_{b,\vec{q}}$ are the electron-phonon couplings. We include here polar coupling to longitudinal optical phonons and deformation potential coupling to acoustic phonons.

In the BTE [8] the electron wave functions are plane waves with a characteristic momentum $\langle\vec{p}\rangle = \hbar\vec{k}$. Electron-phonon scattering rates are calculated with Fermi's golden rule. While such calculations yield long scattering times (≈ 200 fs) for electrons near the conduction band minimum, the scattering times decrease markedly for electrons able to scatter into side valleys (L and X). Very short times (down to 3 fs) are obtained for electrons in the negative mass regions. With such short scattering times it would be impossible on our time scale (100 fs) to have ballistic transport across these regions. Instead, one would expect that nearly all electrons are scattered into the side valleys, where they would remain for the rest of the pulse [15], before reaching the negative mass regions. Since electrons in the side valleys have rather low velocities (<200 km/s) [8,16], scattering into the side valleys would result in a drastic reduction of the electron velocity and thus of the emitted field. Accordingly, one expects a strong

signal $E_{em}(t)$ at the beginning of the pulse, but only very weak signals at later times [dash-dotted line in Fig. 3(f)]. This is obviously not what is observed.

Our theory to describe high-field transport on short time scales is an extension of [10,17]. In contrast to the BTE, we solve the full Schrödinger equation of the electron-phonon system approximatively. We assume that the electrons are described by spherical bandwidth-limited Gaussian wave packets with $\Delta x^2 = \langle x^2 \rangle - \langle x \rangle^2 = \hbar^2/4\Delta p_x^2$ and $\Delta p_x^2 = \Delta p_y^2 = \Delta p_z^2$. The expectation values of the kinetic energy $\langle \mathcal{E}(\vec{p}) \rangle = \mathcal{E}_{kin}(\langle p_x \rangle, \Delta p_x^2)$ and of the velocity operator $\langle v_x \rangle = \mathcal{V}_x(\langle p_x \rangle, \Delta p_x^2)$ are functions of both $\langle p_x \rangle$ and Δp_x^2. We obtain the following system of equations:

$$\frac{d\langle x \rangle}{dt} = \langle v_x \rangle = \mathcal{V}_x(\langle p_x \rangle, \Delta p_x^2), \qquad (5)$$

$$\frac{d\langle p_x \rangle}{dt} = -eE(t) + \sum_{b,\vec{q}} \exp(-\vec{q}^2 \Delta x^2/2) M_{b,\vec{q}}$$
$$\times [\langle P_{b,\vec{q}} \rangle q_x \sin q_x \langle x \rangle - \omega_{b,\vec{q}} \langle Q_{b,\vec{q}} \rangle q_x \cos q_x \langle x \rangle], \quad (6)$$

$$\frac{d\langle Q_{b,\vec{q}} \rangle}{dt} = \langle P_{b,\vec{q}} \rangle + M_{b,\vec{q}} \cos q_x \langle x \rangle \exp(-\vec{q}^2 \Delta x^2/2), \quad (7)$$

$$\frac{d\langle P_{b,\vec{q}} \rangle}{dt} = -\omega_{b,\vec{q}}^2 \langle Q_{b,\vec{q}} \rangle - M_{b,\vec{q}} \omega_{b,\vec{q}} \sin q_x \langle x \rangle$$
$$\times \exp(-\vec{q}^2 \Delta x^2/2), \qquad (8)$$

$$\frac{d\Delta p_x^2}{dt} = \left[\frac{\partial \mathcal{E}_{kin}(\langle p_x \rangle, \Delta p_x^2)}{\partial \Delta p_x^2}\right]^{-1} \left\{ \mathcal{V}_x(\langle p_x \rangle, \Delta p_x^2) \right.$$
$$\times \sum_{b,\vec{q}} \exp(-\vec{q}^2 \Delta x^2/2) M_{b,\vec{q}} [\langle P_{b,\vec{q}} \rangle q_x \sin q_x \langle x \rangle$$
$$- \omega_{b,\vec{q}} \langle Q_{b,\vec{q}} \rangle q_x \cos q_x \langle x \rangle] + \Gamma_{loss}(p_x, \Delta p_x^2, T_L)$$
$$\left. \times [\mathcal{E}_{kin}(\langle p_x \rangle, m_{eff} k_B T_L) - \mathcal{E}_{kin}(\langle p_x \rangle, \Delta p_x^2)] \right\}. \quad (9)$$

Emission and absorption of incoherent phonons are described by the energy relaxation rate $\Gamma_{loss}(p_x, \Delta p_x^2, T_L)$, which is low enough [8] that it can be calculated by Fermi's golden rule. In the absence of external electric fields this term relaxes the wave-packet size to its value at thermal equilibrium, $\Delta p_x^2 = m_{eff} k_B T_L$. Eqs. (5)–(8) are similar to those of the classical polaron [18]. The main difference stems from the finite wave-packet size $\Delta x^2 = \hbar^2/4\Delta p_x^2$ [Eq. (9)]. This size determines the friction forces acting on the electron, since only phonons with $\vec{q}^2 < 1/\Delta x^2$ can couple efficiently [Eq. (6)]. Thus, for large wave packets the friction is weak, leading to ballistic transport, for small ones the friction is strong, leading to drift transport. In our experiment, we start with a large wave packet corresponding to a small Δp_x^2. To increase Δp_x^2, incoherent energy has to be supplied by the friction force [Eq. (9)], which takes several 100 fs, leading on

ultrafast time scales to negligible changes of Δp_x^2 and, thus, to ballistic transport. This behavior originates from quantum-kinetic memory effects in the electron-phonon interaction. Theoretical results for $E < 80$ kV/cm [17,19] have shown that energy nonconserving transitions lead to interferences between the electron–electric-field and the electron-phonon interaction. Our experiments and simulations confirm this trend for much higher fields.

Outside the quantum-kinetic regime our dynamic polaron theory and the semiclassical BTE [8] give identical results, e.g., for the stationary drift velocity in high fields [Fig. 1(b)]. For the long times inherent in stationary transport, enough energy can be supplied to the polaron to decrease its wave-packet size to very low values [20], leading to strong friction forces and thus to drift transport [16].

To conclude, we have observed ballistic transport of electrons in GaAs across half the Brillouin zone by time-resolved high-field THz measurements. We present a model for high-field transport using polarons that agrees with our experimental results on short time scales and yields the correct drift velocity on long time scales.

[1] F. Bloch, Z. Phys. **52**, 555 (1929).
[2] J. R. Chelikowsky and M. L. Cohen, Phys. Rev. B **14**, 556 (1976); **30**, 4828 (1984).
[3] B. K. Ridley, *Quantum Processes in Semiconductors* (Oxford University Press, Oxford, 1993), 3rd ed.
[4] J. Feldmann *et al.*, Phys. Rev. B **46**, 7252 (1992); C. Waschke *et al.*, Phys. Rev. Lett. **70**, 3319 (1993); K. Unterrainer *et al.*, *ibid.* **76**, 2973 (1996).
[5] I. Bloch, Nature (London) **453**, 1016 (2008).
[6] J. Delahaye *et al.*, Science **299**, 1045 (2003).
[7] D. N. Christodoulides, F. Lederer, and Y. Silberberg, Nature (London) **424**, 817 (2003).
[8] M. V. Fischetti, IEEE Trans. Electron Devices **38**, 634 (1991).
[9] P. Gaal *et al.*, Phys. Rev. B **77**, 235204 (2008).
[10] P. Gaal *et al.*, Nature (London) **450**, 1210 (2007).
[11] K. Reimann, Rep. Prog. Phys. **70**, 1597 (2007).
[12] T. Shih *et al.*, Phys. Rev. B **72**, 195338 (2005).
[13] A. Leitenstorfer *et al.*, Phys. Rev. B **61**, 16642 (2000).
[14] T. D. Lee, F. E. Low, and D. Pines, Phys. Rev. **90**, 297 (1953).
[15] T. Tsuruoka, H. Hashimoto, and S. Ushioda, Thin Solid Films **464–465**, 469 (2004).
[16] T. H. Windhorn *et al.*, Appl. Phys. Lett. **40**, 513 (1982); M. Abe *et al.*, *ibid.* **81**, 679 (2002).
[17] W. Magnus and W. Schoenmaker, Phys. Rev. B **47**, 1276 (1993).
[18] L. Bányai, Phys. Rev. Lett. **70**, 1674 (1993).
[19] F. Rossi and C. Jacoboni, Semicond. Sci. Technol. **7**, B383 (1992).
[20] J. H. Jensen and J. A. Sauls, Phys. Rev. B **38**, 13387 (1988).
[21] J. B. Gunn, Solid State Commun. **1**, 88 (1963).